Preprints of the 19th World Congress
The International Federation of Automatic Control
Cape Town, South Africa. August 24-29, 2014

Controlling A Motion Platform Beyond Its Anti-Resonance

Evrim Onur Ari * **Erol Kocaoglan** **

* *Unmanned Systems Department, Aselsan Inc. Defense System Technologies Division Ankara - Turkey*
Tel:90-312-5922548 (e-mail: oari@aselsan.com.tr)
** *Department of Electrical and Electronics Engineering Middle East Technical University Ankara - Turkey*
Tel:90-312-2102367 (e-mail: erolkoc@metu.edu.tr)

Abstract: In controlling motion platforms,the servo motor and the feedback sensor are in general, not co-located. Hence, there usually happens to be a mechanical anti-resonance in controlling the system in velocity mode. This anti-resonance hinders the controller design as the open-loop gain of the system is severely reduced. In this study, a novel approach based on self-recurrent wavelet neural networks (SRWNNs) has been proposed in order to re-shape the anti-resonance behavior of the open-loop plant in a robust manner. The approach has been verified both using simulations and experiments.

Keywords: Servo systems, motion platforms, wavelet neural networks, adaptive control.

1. INTRODUCTION

Motion platforms with payloads are widely used in modern defense systems (e.g. Fig. 1). In most of these systems platform actuation is achieved by driving brushless electric motors via power electronic components. These components are controlled by processors using feedback information from several sensors. The aim of control is generating "the correct motor current" which will move the platform with desired speed with respect to earth reference frame. Hence, the control tries to suppress the disturbances (hull motion, windage , sea waves etc.) while trying to obtain a closed loop transfer function from reference command to load speed equal to or at least very close to unity.

In modeling motion platforms for control purpose, the system is usually divided into two parts as "electrical" and "mechanical" subsystems. The electrical sub-system does usually have a wider bandwidth and under certain conditions it can simply be modeled as unity or as a simple first-order low-pass filter Ari [2013]. The mechanical part of the motion platform is usually modeled as a multi-body system with elastic connections in between. Usually mechanical model with three inertias is sufficient for the purpose of control, while models with two inertias are also common.

A typical three inertia model with elastic connections is shown in Fig. 2. Control of such mechanical systems have been widely studied during past 40 years. In what follows, a few of these studies are mentioned: In Yuki [1993] resonance ratio control concept is introduced. In this concept, an observer is used in order to sense the reaction torque information between the rigid bodies; and then, this information is employed in order to produce additional motor torque via observer feedback. In Zhang [1999] a linear system model consisting of two rigid inertias connected via a spring that represents the finite stiffness of the overall structure is employed. PI and PID controllers for such a system are designed by analyzing the closed-loop system pole locations in terms of controller and plant parameters. In this study, it is shown that controller parameters cannot independently adjust all the pole locations, instead one must compromise between damping and natural frequencies of the poles while tuning the PI controller. In Zhang [1999] the same authors consider the extension of their method to a three-inertia system model. The relationship between system parameters (inertia distribution, stiffness etc.) and controller complexity is investigated and parameter plane method is employed in order to determine a regulatory PI controller's parameters in terms of system parameters and closed-loop performance specifications. In Ji [1995] a full-state feedback LQR controller was proposed for the speed control of a two-mass system, where the states are observed by employing a Kalman Filter. In O'Sullivan [2006], in order to perform resonance ratio control (RRC) surface-acoustic wave (SAW) torque

Fig. 1. An example of a stabilized motion platform: Pedestal Mount Stinger Launching System - PMS ATILGAN® (Photo Courtesy of Aselsan Inc.)

Copyright © 2014 IFAC

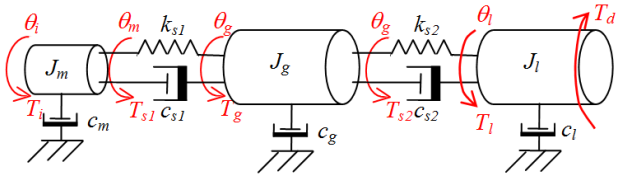

Fig. 2. Typical 3 mass model schematic of a motion platform.

transducers are employed as feedback elements. PI, PID and RRC controller performances are compared and it is shown that ,in terms of disturbance rejection, PID and RRC controllers are identical. In order to improve performance of RRC controller a new alternative termed as RRC+ is proposed. In this method, derivative of the measured motor shaft torque is employed as a feedback term in the controller. In Ellis [2000] several methods that could be used for control of a resonant system has been investigated. These methods are usage of a low-pass filter, a notch filter or a bi-quad filter for the suppression of the resonance; and compliant-body and rigid body observers for acceleration feedback (corresponding to RRC), active resonance damping and center of mass control. Among the filters, the low-pass filter is stated to be lagging the phase at lower frequencies and the notch and the bi-quad filters are found to be non-robust. Usage of clsoed loop observers (with forms similar to a Luenberger Observer) for acceleration feedback was found to be the best method among the considered ones in terms of closed-loop bandwidth. In Ellis [2001], observer design is analyzed in more detail and FRF of closed-loop performances are given, expressing that acceleration feedback obtained from a closed-loop observer is both more robust and it allows higher closed-loop bandwidth. In Szabat [2007] it is summarized that the two-mass lumped system state-feedbacks can be grouped in three different categories. With only one feedback, a classical PI controller can only control one free parameter of the closed loop system dominant pole: either damping or natural frequency. In order to control both damping and resonant frequency at least two feedbacks from two different categories must be employed. There also have been more "modern" approaches employed for multi-body system control similar to H_∞,neural networks, fuzzy control, model predictive control. But very common drawbacks of these methods are design complexity and/or parameter convergence problems. The examples for multi-body elastic system control may be extended further. There are also several studies on modeling and control of non-linear effects dominating such systems (backlash, friction etc.). However, since we have a limited space, we leave further literature survey to the reader and focus on our control approach.

This paper is organized as follows: In section 2, the system model is revisited and the major properties of the model in terms of its parameters are given. In section 3, The details of the controller architecture employed in the study are given. Section 4 gives the simulation results. Section 5 is dedicated to experimental evaluation of the performance of the proposed architecture. The paper ends with conclusions.

2. SYSTEM MODEL

The schematic of a typical system model for a three-mass system is shown in Fig. 2. The parameters used in this figure are summarized in Table 1.

Table 1. Parameters of the 3-mass system given in Fig. 2

PARAMETER	UNIT	REMARKS
T_m	Nm	Input Motor Torque
T_d	Nm	Equivalent Disturbance Torque
θ_m	rad	Motor Shaft Position
θ_g	rad	Second Mass Position
θ_l	rad	Third Mass Position
c_m	Nm.s/rad	Motor Shaft Bearing Viscosity
c_g	Nm.s/rad	Second Mass Bearing Viscosity
c_l	Nm.s/rad	Third Mass Bearing Viscosity
c_{si}	Nm.s/rad	i^{th} Joint Viscosity
k_{si}	Nm/rad	i^{th} Joint Stiffness
J_m	kgm^2	First Mass Inertia
J_g	kgm^2	Second Mass Inertia
J_l	kgm^2	Third Mass Inertia

2.1 Transfer Function Evaluation

One can easily derive a linear MIMO model for such a system by writing down the equations of motion for each body, taking the Laplace transforms of the resulting equations, and finally solving for inertia speeds in terms of input torques (being the motor and disturbance torques). This process results in the following MIMO transfer function model:

$$\begin{bmatrix}\Omega_m(s)\\ \Omega_g(s)\\ \Omega_l(s)\end{bmatrix} = \frac{s}{\Delta}\begin{bmatrix}(D^2-CE) & BD\\ -BE & AD\\ -BD & (AC-B^2)\end{bmatrix}\begin{bmatrix}T_m(s)\\ T_d(s)\end{bmatrix} \quad (1)$$

with

$$A = J_m s^2 + (c_m + c_{s1})s + k_{s1} \quad (2)$$

$$B = c_{s1}s + k_{s1} \quad (3)$$

$$C = J_g s^2 + (c_g + c_{s1} + c_{s2})s + k_{s1} + k_{s2} \quad (4)$$

$$D = c_{s2}s + k_{s2} \quad (5)$$

$$E = J_l s^2 + (c_l + c_{s2})s + k_{s2} \quad (6)$$

$$\Delta = B^2E + AD^2 - ACE \quad (7)$$

and $\Omega_m(s), \Omega_g(s)$, $\Omega_l(s)$, $T_d(s)$ and $T_m(s)$ representing Laplace transforms of $\omega_m(t), \omega_g(t)$, $\omega_l(t)$,$T_d(t)$ and $T_m(t)$ respectively.

In most of the previous studies the concern had usually been the control of the motor speed ω_m (Yuki [1993],Zhang [1999] etc.) or the control of the load speed ω_l (Ellis [2001],Szabat [2007] etc.). However, our concern is controlling the second mass speed (i.e. ω_g). This is since, in most

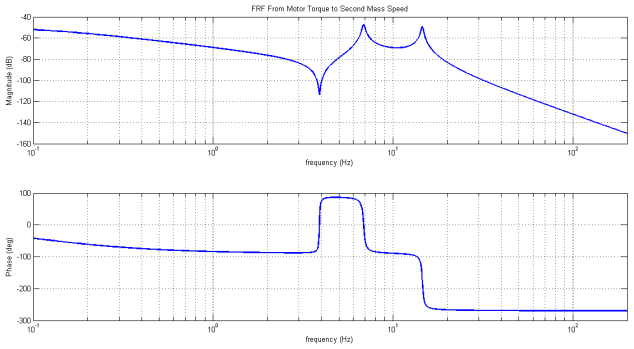

Fig. 3. Typical Frequency Response Function (FRF) plot for the second mass speed output of a 3 mass system.

of the motion platforms, the sensor used for measuring the angular speed is placed in between the motor (or actuator) and the load. Representing the motor as the first mass (J_m) and representing the load as the third mass (J_l) the most appropriate way of representing the dynamics of the sensor speed is to place another mass (J_g) between these two masses.

2.2 Some Remarks on Frequency Domain Behaviour

When we investigate the frequency response function

$$G_{gm}(j\omega) = \frac{\Omega_g(j\omega)}{T_m(j\omega)} \tag{8}$$

we see that its behavior is dependent on the values of the system parameters given in Table 1. The mechanical modes of the system are functions of stiffness and inertia values, while mode damping values are highly dependent on viscosity terms. For a typical motion platform (i.e. with $J_l >> J_m$ and $k_{s2} << k_{s1}$) the frequency response function defined in (8) is similar to the one given in Fig. 3. If we investigate this figure, it is easily seen that we have an anti-resonance at a lower frequency than resonances. In order to deal with this anti-resonance, the controller must have a very high gain at least in the close neighborhood of this frequency. On the other hand, in order to have a large enough gain margin, the open-loop FRF must be far less than 0 dB whenever the phase lag is $-180°$. Hence the controller must suppress the resonances shown in Fig. 3. Finally, in order not to have a spillover effect, which may be defined as the instability caused by higher frequency modes which are not modeled, the controller must suppress the high frequency content. In order to achieve such a performance several notch or bi-quad filter designs are proposed (Ellis [2000]). Moreover the anti-resonance effect can simply be dealt with poles placement (Ellis [2001]) by employing the method of Truxal and Guillemin. However, it is very well known that, without using additional sensors (not practical for our case) and take precautions for avoiding instability, these methods are simply not robust and makes the system unstable in practice. Hence, we need a control architecture which gives high gains in the vicinity of the anti-resonance frequency; suppresses the response about the resonance frequencies and adapts itself accordingly in the case that these critical frequencies somehow shift during operation.

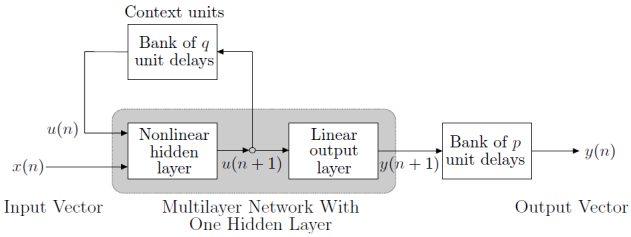

Fig. 4. Recurrent Neural Network in State-Space Model form. (Veitch [2005])

3. PROPOSED CONTROL ARCHITECTURE

3.1 SRWNN Structure Used

Wavelet Neural Networks (WNNs) are neural networks in which neurons' activation functions are wavelets. The main advantage of WNNs with respect to the standard NNs is that they converge faster. Moreover, employing concepts from MRA, WNNs are able to mimic dynamic system behaviour with very high performance when used in recurrent form as given in Fig. 4. Such a neural network is literally termed as a "Self-Recurrent Wavelet Neural Network".

The SRWNN structure used in this study was proposed in Yoo [2005]. As seen in Fig. 5 this structure consists of mainly four layers:

- Layer 1: The input layer.It consists of N_i nodes representing inputs to the SRWNN.
- Layer 2: The mother wavelet layer. It consists of N_w wavelon groups each having N_i wavelons corresponding to every element of the input vector of the SRWNN. k^{th} wavelon of the j^{th} wavelon group performs the following calculation

$$\phi_{jk}(z_{jk}) = \phi(\frac{u_{jk} - m_{jk}}{d_{jk}}) \tag{9}$$

where

$$z_{jk} = \frac{u_{jk} - m_{jk}}{d_{jk}}, u_{jk}(n) = x_k(n) + \phi_{jk}(n-1)\theta_{jk} \tag{10}$$

In (9) and (10), x_k denotes the k^{th} element of the input vector; m_{jk}, d_{jk} and θ_{jk} denote the translation, dilation and feedback gain of the wavelon jk , respectively.
- Layer 3: The product layer. It consists of N_w product elements. j^{th} product element merges the corresponding mother wavelet group activation as

$$\Phi_j(x) = \prod_{k=1}^{N_i} \phi(z_{jk}) \tag{11}$$

- Layer 4: The output layer: Consists of a summer and calculates the output as

$$y = \sum_{j=1}^{N_w} w_j \Phi_j(x) + \sum_{k=1}^{N_i} a_k x_k \tag{12}$$

where w_j is the weight of the j^{th} wavelon group, and a_k is the weight of the k^{th} input vector element. Note that, in (12) the second sum denotes a linear component between the input and the output,

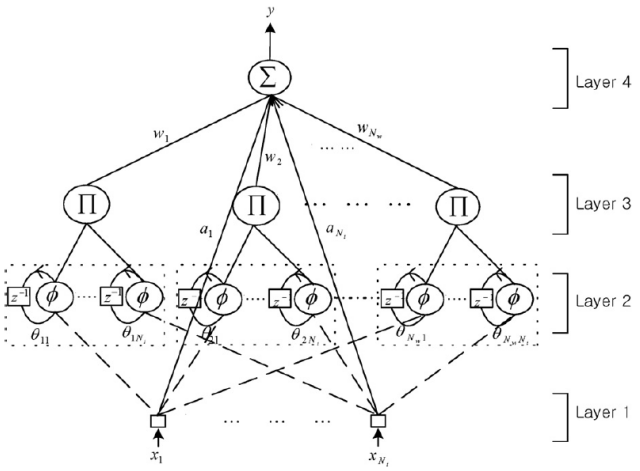

Fig. 5. SRWNN internal structure proposed in Yoo [2005]

which behaves similar to a proportional controller. In Alizadeh [2013] this part is not used, but the SRWNN itself replaces the proportional part of a PID controller.

3.2 Modified Adaptive Learning Rates (MALR)

The SRWNN structure given in Fig. 5 is an adaptive structure, whose weight vector is defined as

$$\boldsymbol{W} = [\boldsymbol{a}\ \boldsymbol{m}\ \boldsymbol{d}\ \boldsymbol{\theta}\ \boldsymbol{w}] \tag{13}$$

$\boldsymbol{W}$ is adapted according to the gradient descent algorithm, which is described by

$$\boldsymbol{W}(n+1) = \boldsymbol{W}(n) - \bar{\eta}\nabla_W J \tag{14}$$

where $\bar{\eta}$ is the diagonal matrix of learning rates,$\bar{\eta} = diag(\eta^a, \eta^m, \eta^d, \eta^\theta, \eta^w)$, and $\nabla_W J$ denotes the gradient of the cost function J with respect to the weights vector $\boldsymbol{W}$. Cost function is usually quadratic and it's in the form

$$J(n) = \frac{1}{2}[y_d(n) - y(n)]^2 = \frac{1}{2}e^2(n) \tag{15}$$

where $y_d(n)$ is the desired output at time step n. The above definition of cost function results in

$$\nabla_W J = -e(n)\nabla_W y \tag{16}$$

where the term $\nabla_W y$ can be easily evaluated by applying the chain rule for each weight vector entry. The details of the results are given in Yoo [2005].

A set of adaptive upper bounds η^* for learning rates have been proposed in Yoo [2005]. However, the approach used in finding the bounds is for making sure the convergence of SRWNN at all times, rather than the speed of convergence. Hence we slightly modified the adaptive learning rate algorithm as given below:

$$\eta(n) = \begin{cases} \eta^*, & \text{if } n > n^* \\ \eta^K, & \text{if } n < n^* \end{cases} \tag{17}$$

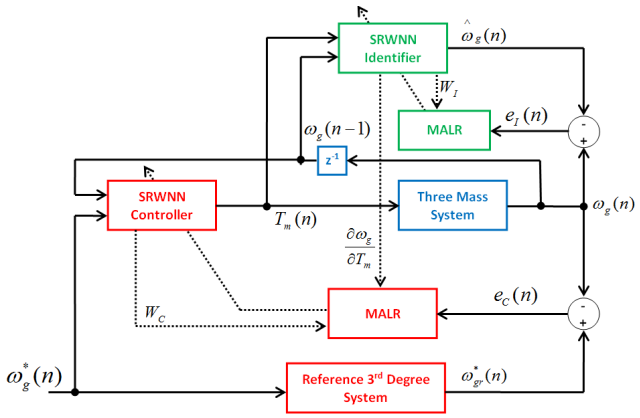

Fig. 6. SRWNN based iterative adaptive controller (SRWNN IAC) structure similar to the one in Yoo [2007].

where η^* is the adaptive learning rate, calculated as in Yoo [2005]. i.e. ,at the beginning of the adaptation process, by keeping higher learning rates, the process of learning is accelerated. The values for η^K and n^* might be determined experimentally.

3.3 Control Architecture

SRWNN structure has been used in various architectures for control purpose. These include predictive control (Yoo [2005]),indirect adaptive control (Yoo [2007]),as the proportional part of a standard PID controller(Alizadeh [2013]). In this study, we use the indirect adaptive control architecture (Yoo [2007]) with modified learning rate update algorithms. The general structure of indirect adaptive control is shown in Fig. 6.

The majority of similar studies (e.q. Kowalska [2007]) use a second order linear system model as the reference for the closed-loop. In this study, we keep in mind that, for a linear pole-placement approach, for the controller to be realizable, the pole excess of the closed-loop system must be larger than or equal to the pole excess of the plant itself. Since our plant has 3 excessive poles, we use a reference model with three excessive poles. We put triple poles to a frequency higher than the anti-resonance (see Fig. 3), and set the DC gain to unity by adding a constant to the numerator, which results in

$$G_R(s) = \frac{60^3}{(s+60)^3} \tag{18}$$

Another issue in this control architecture is that the gradient given in (16) cannot be used directly since we have the cost function given as

$$J(n) = \frac{1}{2}[\omega_{gr}^*(n) - \omega_g(n)]^2 = \frac{1}{2}e_C^2(n) \tag{19}$$

By applying chain rule we can write

$$\nabla_W J = -e_C(n)\frac{\partial \omega_g}{\partial T_m}\nabla_W T_m \tag{20}$$

where the $\nabla_W T_m$ term can be easily found by the chain rule, as stated before. However, the sensitivity term given

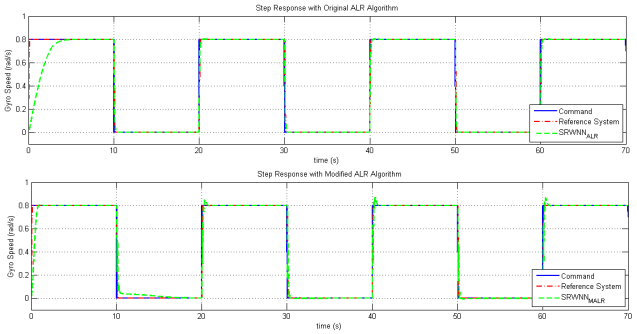

Fig. 7. Step Response with the original ALR algorithm (top) and the Modified ALR algorithm (bottom).

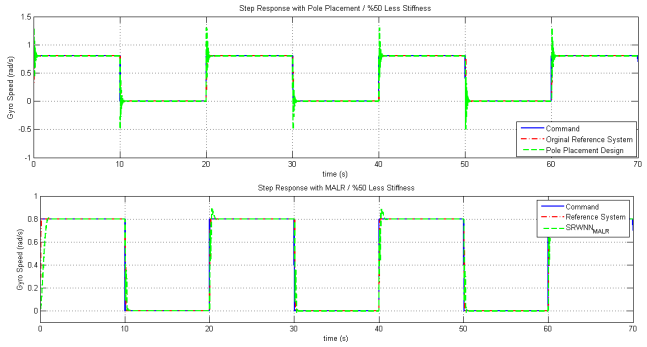

Fig. 8. Step Response when stiffness values are reduced by 50%. The Truxal-Guillemin design(top) and SRWNN IAC (bottom).

by $\frac{\partial \omega_g}{\partial T_m}$ cannot be calculated directly. For this reason, we utilize the approach given in Yoo [2007] and incorporate an SRWNN identifier into the architecture, in which the term $\frac{\partial \omega_g}{\partial T_m}$ can be calculated by the chain rule easily (see Fig. 6 and Yoo [2007] for details).

4. SIMULATIONS

Table 2. Performance Comparison

Algorithm	SRWNN MALR	SRWNN ALR	3^{rd} Order Reference	PI
t_{conv} convergence time	0.83s	4.3s	N/A	N/A
t_s settling time	0.18s	0.18s	0.13s	0.72s
t_r rise time	0.14s	0.14s	0.07s	0.54s
M_O max. overshoot	8%	1%	0	0
t_{Iconv} identifier convergence time	1.2s	2.1s	N/A	N/A

During simulations a three mass system linear model is employed as the plant. A square wave speed command reference has been applied to the system. SRWNN structures with $N_w = 4$ has been utilized for both the identifier and the controller. The results for step response is shown in Fig. 7. In this figure, it is seen that when the SRWNN IAC is utilized with the standard adaptive learning algorithm, it takes around 4.3 seconds for the system to follow the command. But with the modified learning rate algorithm

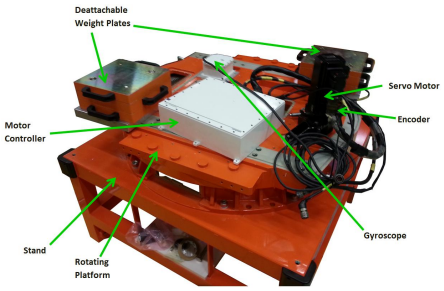

Fig. 9. Test setup on which experiments have been conducted.

it takes 0.83 seconds. The numerical figures from the simulations and experiments has been summarized in Table 2.

The robustness performance of the SRWNN IAC is tested by reducing the stiffness values by a factor of 0.5 during the simulation. As expected, the pole placement (Truxal-Guillemin) design shows under damped oscillatory behavior; while SRWNN IAC controller adapts itself equally well to the new stiffness values as given in Fig. 8.

5. EXPERIMENTS

The setup used during the experiments is given in Fig. 9. This is basically a rotating platform mounted on a stand. It is utilized with a servo motor with 1.4 kW rated power, an Aselsan Herkul® series servo controller capable of delivering up to 14 kWs of instantaneous electrical power to the motor, a gyroscope for inertial speed measurement, an auxiliary encoder for position measurement. Moreover, there are two mechanical interfaces for additional weight plates in order to simulate the load of the motion platform. A PC utilized with MATLAB-RTWT® and capable of communicating with Herkul servo controller is employed for implementation of the controller by hardware in the loop approach.

During the experiments an SRWNN structure with $N_w = 4$ has been employed for both identifier and the controller parts, as in the simulations, with 2 inputs for SRWNN, this sum ups to a total of 30 learning parameters for both SRWNN structures. The comparison between the ALR and the proposed MALR learning rate updates are given in Fig. 10. It is easily observed that the SRWNNI converges to the system output at about 2.1 seconds for ALR, and 1.2 seconds for the MALR case (see Table 2). Note also from the same figure that the system is quite non-linear giving a non-exponential speed output for a square torque input, however SRWNNI structure is complicated enough to capture these non-linearities and find the system sensitivity correctly. The performance of the controller is compared with a high performance PI speed controller as well. The PI controller is tuned so as to have a gain margin of only 2 dBs, making it non-robust but with a high command tracking performance. As seen in Fig. 11 and Table 2, the SRWNN adaptive controller structure outperforms the high performance PI controller in step response with 4 times faster rise time and settling time, and it almost makes the overall system mimic the reference system behaviour. This comes with a trade off of 8% overshoot, however this overshoot may be avoided by

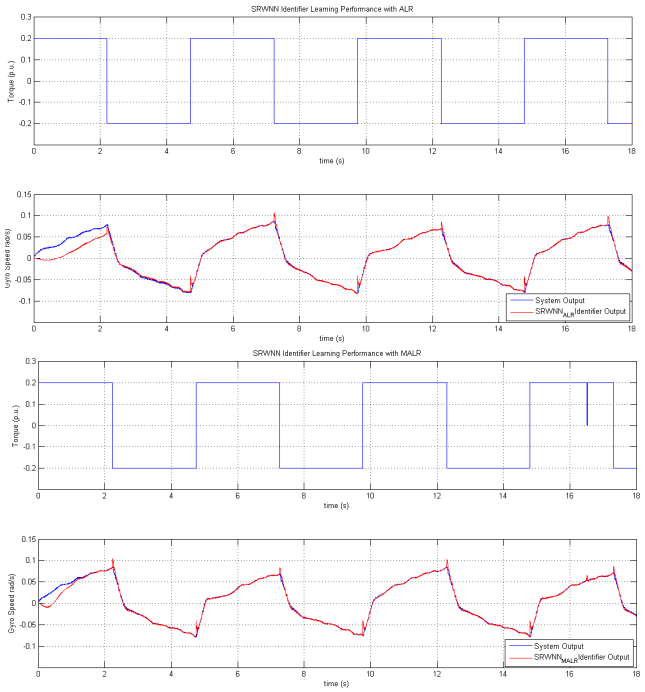

Fig. 10. Experimental result showing the convergence performance of the SRWNN identifier with ALR (top two plots) and MALR (bottom two plots).

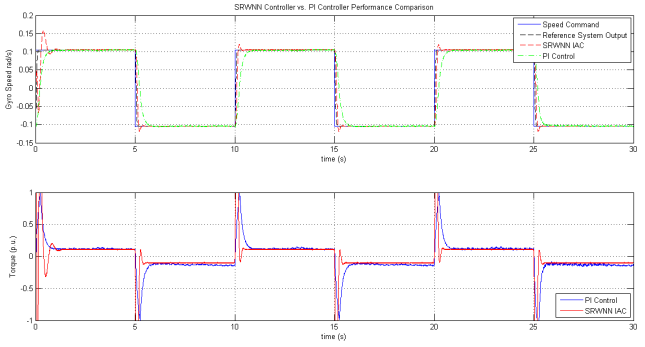

Fig. 11. Experimental results for the comparison of proposed SRWNN IAC and high performance PI controller.

shaping the command in a real system. In addition, notice that: The SRWNN controller saturates the motor torque very rapidly in the case of a step command and uses all the available acceleration of the system in an efficient way; hence using the torque loop bandwidth much more better than the PI controller. We can also state that the main reason for the SRWNN IAC cannot do better in making the system mimic the 3^{rd} order reference system is the actuator saturation (i.e. acceleration limit available).

6. CONCLUSION

In conclusion, the problem of controlling the speed of the second mass in a elastically connected three mass system has been addressed in this paper. A Self-Recurrent Wavelet Neural Network (SRWNN) based controller architecture has been proposed for the solution of the problem so as to achieve a robust performance, while increasing the system bandwidth beyond the anti-resonance frequency of the open-loop system. High performance of the proposed architecture has been verified by both simulations and experiments.

REFERENCES

E.O. Ari and E. Kocaoglan. Investigation of Interactions between Mechanical and Electrical Components of a Motion Platform. *Asian Control Conference Proceedings*, pages 1–6, 2013.

K. Yuki,T. Murakami,K. Ohnishi. Vibration Control of 2 Mass Resonant System by Resonance Ratio Control. *IECON'93 Proceedings*, pages 2009–2014, 1993.

G. Zhang,J. Furusho. Speed Control of Two-Inertia System by PI/PID Control. *International Conference on Power Electronics and Drive Systems*, pages 567–572, 1999.

G. Zhang,J. Furusho. Vibration Control of Three-Inertia System. *IECON'99 Proceedings*, pages 1045–1050, 1999.

J. Ji,S. Sul. Kalman Filter and LQ Based Speed Controller for Torsional Vibration Suppression in a 2-Mass Motor Drive System. *IEEE Transactions on Industrial Electronics*, Vol. 42, No. 6, pages 564-571, 1995.

T.M. O'Sullivan,C.M. Bingham,N. Schofield. High-Performance Control of Dual-Inertia Servo-Drive Systems Using Low-Cost Integrated SAW Torque Transducers. *IEEE Transactions on Industrial Electronics*, Vol. 53, No. 4, pages 1124–1132, August 2006.

G. Ellis,R.D. Lorenz. Resonant Load Control Methods for Industrial Servo Drives. *Industry Applications Conference Proceedings*,vol. 3, pages 1438–1445, 2000

G. Ellis,Z. Gao. Cures for Low-Frequency Mechanical Resonance in Industrial Servo Systems. *Industry Applications Conference Proceedings*,vol. 1, pages 252–258, 2001

K. Szabat,T. Orlowska-Kowalska. Vibration Suppression in a Two-Mass Drive System Using PI Speed Controller and Additional Feedbacks - Comparative Study. *IEEE Transactions on Industrial Electronics*, Vol. 54, No. 2,pages 1193–1206 ,April 2007.

J.C. Goswami,A.K. Chan. Fundamentals of Wavelets: Theory, Algorithms and Applications. *Wiley Series in Microwave and Optical Engineering*, 1999.

D. Veitch. Wavelet Neural Networks and Their Application in the Study of Dynamical Systems. *Department of Mathematics, University of York*, M.Sc. Thesis, August 2005.

S.J. Yoo,J.B. Park,Y.H. Choi. Stable Predictive Control of Chaotic Systems Using Self-Recurrent Wavelet Neural Network. *International Journal of Control, Automation, and Systems*, vol. 3, no. 1, pages 43–55, March 2005.

S.J. Yoo,J.B. Park,Y.H. Choi. Indirect Adaptive Control of Nonlinear Dynamic Systems . *Information Sciences*, vol. 177, issue 15, pages 3074–3098, August 2007.

M. Alizadeh,S. Ganjefar,M. Alizadeh. Wavelet Neural Adaptive Proportional Plus Conventional Integral-Derivative Controller Design of SSSC for Transient Stability Improvement. *Engineering Applications of Artificial Intelligence*, vol. 26, issue 9, pages 2227–2242, October 2013.

T. Kowalska,K. Szabat. Control of the Drive System with Stiff and Elastic Couplings Using Adaptive Neuro-Fuzzy Approach. *IEEE Transactions on Industrial Electronics*, vol. 54, issue 1, pages 228–240, February 2007.